

# Ultrafast Laser Writing in Different Types of Silica Glass

Yuhao Lei,\* Huijun Wang, Linards Skuja, Bodo Kühn, Bernhard Franz, Yuri Svirko, and Peter. G. Kazansky\*

It is demonstrated that ultrafast laser writing in silica glass depends on the grade of silica glass associated with the method of its manufacture. Moreover, laser-written modifications, in particular birefringent modifications, reveal a dependence on the geometry of writing, that is, the modification strength of voxels is smaller than that of single line structures and multi-line scanned areas, which can be explained by free carrier diffusion and reduced electric field in scanning writing. The retardance of scanned birefringent region produced in the regime of anisotropic nanopores formation in silica glass manufactured by vapor axial deposition (VAD) is about five times higher than that in an electrically fused sample at the same laser writing parameters, while the difference in retardance of a nanograting based modification in synthetic and fused silica is only about 10%. The phenomenon is interpreted in terms of the higher concentration of oxygen deficient centers in the electrically fused silica glass, which can confine self-trapped holes and prevent the nanopores formation. Improvement of high transmission optical elements is demonstrated in the VAD sample, and low cost multiplexed optical data storage with higher capacity and readout accuracy is realized in the electrically fused silica glass.

## 1. Introduction

In the last few decades, the interaction of intense ultrashort light pulses with transparent materials has attracted considerable interest due to new phenomena associated with light-induced modification of materials and applications ranging from laser surgery,<sup>[1]</sup> three-dimensional (3D) integrated optics,<sup>[2–4]</sup> microfluidics,<sup>[5–7]</sup> and optical data storage.<sup>[8,9]</sup> In transparent media, femtosecond laser pulses, unlike longer pulses, can deposit energy rapidly and precisely via nonlinear absorption. Among the various materials, ranging from glasses<sup>[10–13]</sup> to crystals,<sup>[14,15]</sup> that are used in ultrafast laser writing, silica glass<sup>[16–18]</sup> is one of the most studied due to its wide ultraviolet (UV) to infrared (IR) transmission range, high chemical resistance, thermal stability, and high optical damage threshold.<sup>[19]</sup> Nonlinear absorption of intense ultrashort light pulses in silica glass can produce a variety of modifications from refractive index

increase (referred as type 1)<sup>[20]</sup> to birefringent modification via formation of polarization-controlled periodic lamella structures or nanogratings (referred as to type 2).<sup>[21,22]</sup> Birefringence patterning can be used to create geometric phase optics elements (GPOEs) and polarization or vector beam converters<sup>[23]</sup> with applications ranging from generating extreme ultraviolet vector beams<sup>[24]</sup> to demonstrating spin–orbit interaction of intense light fields.<sup>[25]</sup> Another interesting application of birefringent modification in silica glass is five-dimensional (5D) optical data storage, where three spatial dimensions and two optical dimensions (slow axis orientation and retardance) are exploited to encode information.<sup>[26,27]</sup> Recently, a new type of birefringent modification consisting of flattened nanopores (type X) has been demonstrated in silica glass.<sup>[28]</sup> The main advantage of type X modification is the ultrahigh transmission (>99%) in the visible range, which facilitates ultra-low loss GPOEs and polarization shaping elements,<sup>[28]</sup> and multi-layer 5D data storage.<sup>[29]</sup>

One of the main problems of ultrafast direct laser writing is to increase the speed and accuracy of writing, as well as the strength of material modification at a lower energy cost. In this respect, control of laser beam parameters, including pulse energy, pulse duration, repetition rate, number of pulses and focusing condition have been explored to improve the laser writing efficiency of birefringent structures in silica glass.<sup>[30]</sup> Silica glass

Y. Lei, H. Wang, P. G. Kazansky  
Optoelectronics Research Centre  
University of Southampton  
Southampton SO17 1BJ, UK  
E-mail: yuhao.lei@soton.ac.uk; pgk@soton.ac.uk

L. Skuja  
Institute of Solid State Physics  
University of Latvia  
8 Kengaraga str., Riga LV1063, Latvia  
B. Kühn, B. Franz  
Heraeus Quarzglas GmbH & Co. KG, Photonics – Optics  
Reinhard-Heraeus-Ring 29, 63801 Kleinostheim, Germany

Y. Svirko  
Institute of Photonics, Department of Physics and Mathematics  
University of Eastern Finland  
Joensuu FI-80101, Finland

 The ORCID identification number(s) for the author(s) of this article can be found under <https://doi.org/10.1002/lpor.202200978>

© 2023 The Authors. Laser & Photonics Reviews published by Wiley-VCH GmbH. This is an open access article under the terms of the Creative Commons Attribution License, which permits use, distribution and reproduction in any medium, provided the original work is properly cited.

DOI: 10.1002/lpor.202200978

**Table 1.** Classification, manufacture method, characteristics, and commercial products of silica glass..

	Classification	Manufacture method	Raw materials	Hydroxyl (OH) content [ppm]	Metallic impurities [ppm]	Commercial products
Group A	Type I	Electrical fusion	Pegmatitic quartz sand	<5	<30	Infrasil 301
	Type II	Flame fusion	Quartz crystals	≈150	<30	Herasil 1
	Type III	CVD <sup>a)</sup>	SiCl <sub>4</sub> vapor	<1300	<1	Spectrosil 2000 Corning 7980
	Type III a	OVD <sup>b)</sup>	SiCl <sub>4</sub> vapor	<1	<0.01	Suprasil 300
	Type III b	VAD <sup>c)</sup> with thermal dehydration	SiCl <sub>4</sub> vapor	<20	<0.01	Suprasil 3302 Ohara SK-1310
	Group B		VAD with H <sub>2</sub> Dry VAD			
Type III c		Dry using an organosilicon compound	SiCl <sub>4</sub> vapor	-	-	210BA
Type IV		PCVD <sup>d)</sup>	SiCl <sub>4</sub> vapor	≤ 5	< 1	Suprasil W
F-doped		Synthetic	SiCl <sub>4</sub> vapor	-	-	210B6 (1% F) F7C (3.23% F)

<sup>a)</sup> Chemical vapor deposition; <sup>b)</sup> Outside vapor deposition; <sup>c)</sup> Vapor axial deposition; <sup>d)</sup> Plasma chemical vapor deposition.

is classified into different types according to the manufacturing method, which can lead to variation in its properties, in particular, the ultraviolet and infrared absorption and hydroxyl (OH) concentration.<sup>[19,31]</sup> type I silica glass is fabricated by electrical fusion of pegmatitic quartz sand; type II silica glass is manufactured by flame fusion of natural quartz; type III silica glass is synthesized by hydrolysis of SiCl<sub>4</sub> vapor in an oxygen-hydrogen burner, which is also known as chemical vapor deposition (CVD) method; type IV silica glass is fabricated by pyrolysis of SiCl<sub>4</sub> vapor blow into a plasma burner flame, so called plasma CVD (PCVD) method, in the presence of oxygen. In addition, high purity silica glasses can be fabricated by an outside vapor deposition (OVD, type III a) method or a vapor axial deposition (VAD, type III b) method. No significant difference (within 10%) was observed in the induced refractive index changes, including birefringence based on nanogratings, in the various silica glass grades.<sup>[32]</sup> With respect to doped silica glass, the induced birefringence in Ge-doped silica glass can be stronger or weaker than in pure silica glass depending on writing conditions,<sup>[33,34]</sup> while the birefringence achieved in Ti-doped glass is comparable to that obtained in fused silica.<sup>[35]</sup> Moreover, compared to fused silica, nanogratings with smaller birefringence can be produced by ultrafast laser writing in multicomponent glasses, such as alkali-free aluminoborosilicate glass and borosilicate glass.<sup>[35,36]</sup>

Here we demonstrate the dependence of the isotropic refractive index increase and the induced birefringence produced by ultrafast laser writing on the grade of silica glass. Moreover, we were surprised to observe that the amount of material modification depends on the geometry of the imprinted structure and is different for single voxel, linear, and area structures imprinted by scanning a light beam, which is important to consider when comparing ultrafast laser writing in different materials. The highest birefringence of the nanopore-type modification can be obtained in the purest silica glass samples (type III b) in terms of defects, which is beneficial for the manufacture of elements for geomet-

ric phase optics and polarization shaping. With the same laser writing parameters, the lowest birefringence is observed in electrically fused silica samples (type I), which can be explained by a high concentration of oxygen deficient centers (ODCs). On the other hand, a smaller azimuthal error of birefringent data voxels is achieved in electrically fused silica samples, thereby increasing data capacity and recording speed for 5D optical data storage with lower cost.

## 2. Results and Discussion

Silica glass samples of five different types were used in the experiments (**Table 1**, group A). First, the laser processing parameters (300 fs pulse duration, 0.7 μJ pulse energy, 200 kHz repetition rate, 6 mm s<sup>-1</sup> scanning speed) corresponding to the nanopores-based modification (type X) were chosen. Square areas of 20 μm × 20 μm were imprinted by round-trip raster scanning of a focused light beam with a line spacing of 1 μm and four different polarization azimuths (**Figure 1a**). As expected, the slow axis of the birefringent modification is perpendicular to the polarization of the writing laser beam in all samples, however, the value of retardance of the type X modification exhibits a significant dependence on the grade of silica glass (**Figure 1b**). For the electrically fused silica glass (Infrasil 301), the average retardance is the smallest of about 6 nm, while for the flame fused silica (Herasil 1) sample the retardance value is 10 nm. For two different samples of CVD silica glass, Spectrosil 2000 and Corning 7980, measured retardance values are ≈15 nm. While the OVD sample has the second largest retardance of 20 nm, the largest retardance of 27 nm is found in the VAD samples. In other words, with the same laser parameters, the retardance of type X modification in the VAD samples (Suprasil 3302, Ohara SK-1310) is about two times larger than that of the commonly used CVD silica glasses (Spectrosil 2000, Corning 7980). One of the main applications of

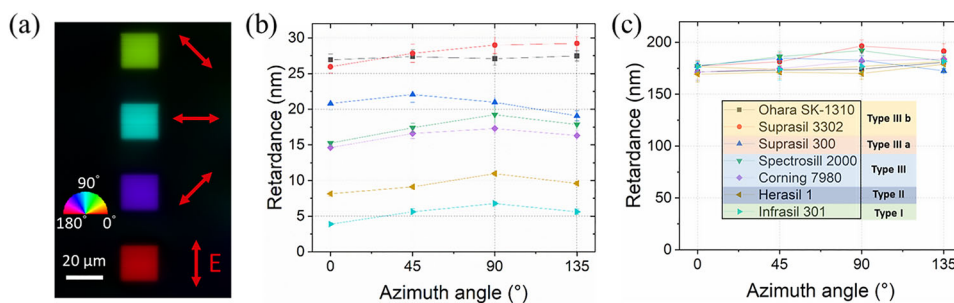


**Figure 1.** Material dependence of birefringent modifications. a) The birefringence image of square type X modifications written by different polarizations. The arrow shows the polarization of the laser beam and pseudo-colors (inset) indicate the local orientation of the slow axis. b,c) Measured retardance of type X and type 2 modifications, respectively, in different silica glasses. Solid lines are guides for the eye. Processing conditions: 0.7  $\mu\text{J}$  pulse energy, 300 fs pulse duration, 6  $\text{mm s}^{-1}$  in (b) or 0.1  $\text{mm s}^{-1}$  in (c) translation speed, and 0.16 NA aspheric lens.

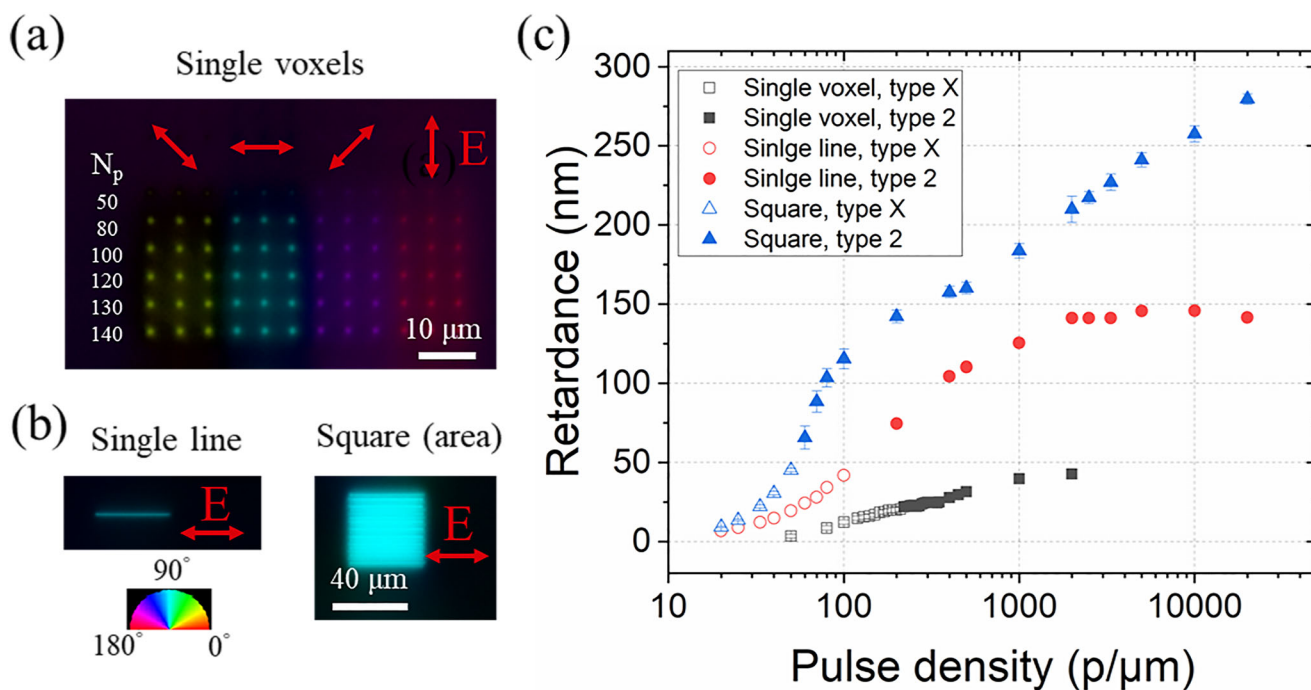


**Figure 2.** Different laser direct writing geometric patterns: a) Single voxel. b) Single line and square (area) generated by the scanning of laser beam. The arrow shows the polarization direction of the writing laser beam and pseudo-colors (inset) indicate the local orientation of the slow axis. c) Measured retardance of type X and type 2 modifications by different birefringent patterning methods versus pulse density. Processing conditions: 0.7  $\mu\text{J}$  pulse energy, 300 fs pulse duration, 0.01  $\text{mm s}^{-1}$  in (a) or 6  $\text{mm s}^{-1}$  in (b) translation speed, and 0.16 NA aspheric lens.

the birefringent modification of the nanopores type is the direct writing of GPOEs and vector beam converters, which requires a multilayer structure with a rather long manufacturing time. These results indicate that VAD silica glasses may be preferable for the fabrication of high transmittance structured birefringent elements. Birefringent structures were also imprinted using laser writing parameters (300 fs pulse duration, 0.7  $\mu\text{J}$  pulse energy, 200 kHz repetition rate, 0.1  $\text{mm s}^{-1}$  scanning speed) corresponding to nanogratings based type 2 modification. In contrast to the type X case, there is no significant difference (within 10%) in the retardance value for different grades of silica glass (Figure 1c), which is consistent with the previous demonstration.<sup>[32]</sup>

The induced birefringence in square areas imprinted by beam scanning was also compared to birefringence in single voxels

and line structures, first in VAD samples (Figure 2). While structures produced by continuous raster scanning are typical in fabrication of birefringent optical elements (Figure 2b), line structures are common in waveguide writing, and voxel structures are used in optical data storage applications (Figure 2a). When writing birefringent voxels, the retardance generally increases with more pulses, peaking at about 20 nm for type X modification, and transforming into type 2 voxels with stronger retardance as the number of pulses increases further (Figure 2c). For line writing, type X retardance increases to about 50 nm with pulse density and transits to type 2 modification when pulse density exceeds 200 pulses  $\mu\text{m}^{-1}$ , after which the retardance increases and reaches saturation at about 140 nm. In raster scanning of the area, the transition from type X modification to type 2

**Table 2.** The maximum retardance of birefringent modifications written by different patterns..

Writing patterns	Type X [nm]	Type 2 [nm]
Single voxel	≈20	≈46
Single line	≈49	≈140
Square (area)	≈50	≈280

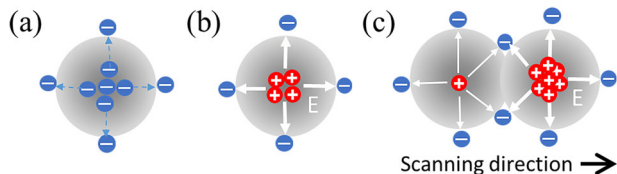


**Figure 3.** The mechanism of material modification by ultrashort light pulses involving generation of free electrons and holes in the photoexcitation region. a) Excitation and diffusion of electrons. b) Generation of holes and built-up electric fields reducing diffusion in stationary writing. c) Reduced electric field and more efficient generation of holes in line writing.

modification is observed at pulse density of 60 pulses  $\mu\text{m}^{-1}$ , while the maximum retardance values reach 50 and 280 nm, respectively (Table 2). The retardance of type X birefringent area also depends on the line separation. For example, when writing with 300 fs pulse duration, 0.7  $\mu\text{J}$  pulse energy, 200 kHz repetition rate, and 6  $\text{mm s}^{-1}$  scanning speed, the retardance of a type X region increases from 27 to 33 nm as the line separation is reduced from 1 to 0.8  $\mu\text{m}$ , while the transition to type 2 modification occurs at a line distance of 0.6  $\mu\text{m}$  (Table S1, Supporting Information).

The maximum retardance ( $\text{Ret.} = \Delta n_b \times l$ ) of the birefringent line structure is as high as 140 nm, which is approximately three times higher than 46 nm we observed in the voxel case. Such a difference in the achievable retardance can be explained if one recalls that the mechanism of material modification by ultrashort light pulses involves nonlinear ionization, that is, generation of free electrons and holes in the irradiated area (Figure 3a). High mobility of free electrons in silica glass and concentration gradient due to the Gaussian profile of the laser beam can result in diffusion of electrons to the beam periphery, in which they are trapped and left behind hardly moveable charged holes in the central region (Figure 3b). The separation of charges due to concentration gradient ( $\nabla n$ ) creates space charges and results in an electric field ( $E_{\text{dc}}$ ) in the irradiated area. Under stationary conditions, ohmic current associated with this field compensates the diffusion current:  $j_{\text{total}} = eD\nabla n - \sigma E_{\text{dc}} = 0$ , where  $e$ ,  $D$  and  $\sigma$  are the electron charge, diffusion coefficient, and conductivity, respectively. When writing a voxel, the concentration of positive holes created by diffusion and trapped in the center of the irradiated region is limited by a circular symmetrical electric field directed from the center to the boundaries of the irradiated region and repelling electrons to the center. In contrast, when writing a line with beam scanning, that is, the laser spot with radius  $R$  is moving with constant velocity  $V$ , the center of the photoexcited region overlaps the boundary of the region, which has already been irradiated at the moment  $\Delta t = R/V$  earlier. This releases the electrons that have been trapped thus reducing the associated space charge and the electric field along the scanning direction, while enhancing charge separation produced by diffu-

sion of free electrons and increasing the concentration of positive holes in the line structure. Alternatively, a line scan can be modeled as a series of closely spaced and overlapping voxel structures. Each voxel will create a space charge field directed oppositely in neighboring voxels, which will lead to a decrease in the resulting space charge field and the associated ohmic current component, as well as to an increase in space charge separation and hole concentration in the central region of the structure (Figure 3c). This effect is further enhanced in the structures produced by area scanning, where not only interface at one side of the voxel, but an interface at a side of a line structure will contribute to the enhancement of charge separation, resulting in the maximum retardance of about two times larger than that for the single line structures. Further, we assume that self-trapped holes behave like polarons and their clustering promotes the formation of nanopores.

When the polarization direction of the writing laser beam is parallel to the scan direction, the maximum retardance of birefringent modification appears. The observed polarization dependent modification strength can be attributed to the anisotropy produced by the interface between modification and pristine material<sup>[37]</sup> or a pulse front tilt of the laser beam (inclination of the intensity front with respect to the propagation direction, PFT).<sup>[38]</sup> In the current experiment, the anisotropy is defined by the scanning direction, which excludes the PFT contribution. The explanation of polarization dependent Fresnel transmission at the interface of modification can be also excluded as in this case modification is expected to be strongest for the polarization perpendicular to the scanning direction.<sup>[39]</sup> We suggest that the nonlinear current driven by the concentration gradient can be responsible for the phenomenon. This current reads  $j_q = \beta_q (\nabla n E) E$ , where  $E$  is the amplitude of the electric field in the linearly polarized excitation beam and  $\beta_q$  is determined by the transport properties of photoexcited electrons in glass. Phenomenologically  $j_q$  can be described in terms of the second-order quadrupole nonlinearity of the glass. The nonlinear current generated by the concentration gradient is directed along the polarization of the light, and the charge separation by this current is maximum when directed along the scanning direction. This current is added to diffusion current generated by the concentration gradient thus strengthening charge separation and dc electric field in the irradiated area:  $eD\nabla n + \beta_q (\nabla n E) E - \sigma E_{\text{dc}} = 0$ . It is worth noting that nonlinear currents are known in glass, and silica glass in particular. For example, the coherent photogalvanic effect, which occurs due to coupling of the fundamental and second harmonic beams, has been observed in silica glass about 20 years ago.<sup>[40,41]</sup>

We also compared writing birefringent modifications using different scanning geometries in different grades of silica glass, in particular, VAD (Ohara SK-1310) and electrically fused (Infrasil 301) samples with the same writing parameters (300 fs pulse duration, 0.7  $\mu\text{J}$  pulse energy, 200 kHz repetition rate, 6  $\text{mm s}^{-1}$  scanning speed). When writing voxels in two samples (Ohara SK-1310 and Infrasil 301), type X modification of different strengths is observed with numbers of pulses from 50 to 200 and nanograting type modification appears when pulse number is increased (Figure 4a). The retardance of type X voxels in the Ohara SK-1310 sample is about two times larger than in the INF 301 sample, the difference of which is not as large as for the area scan

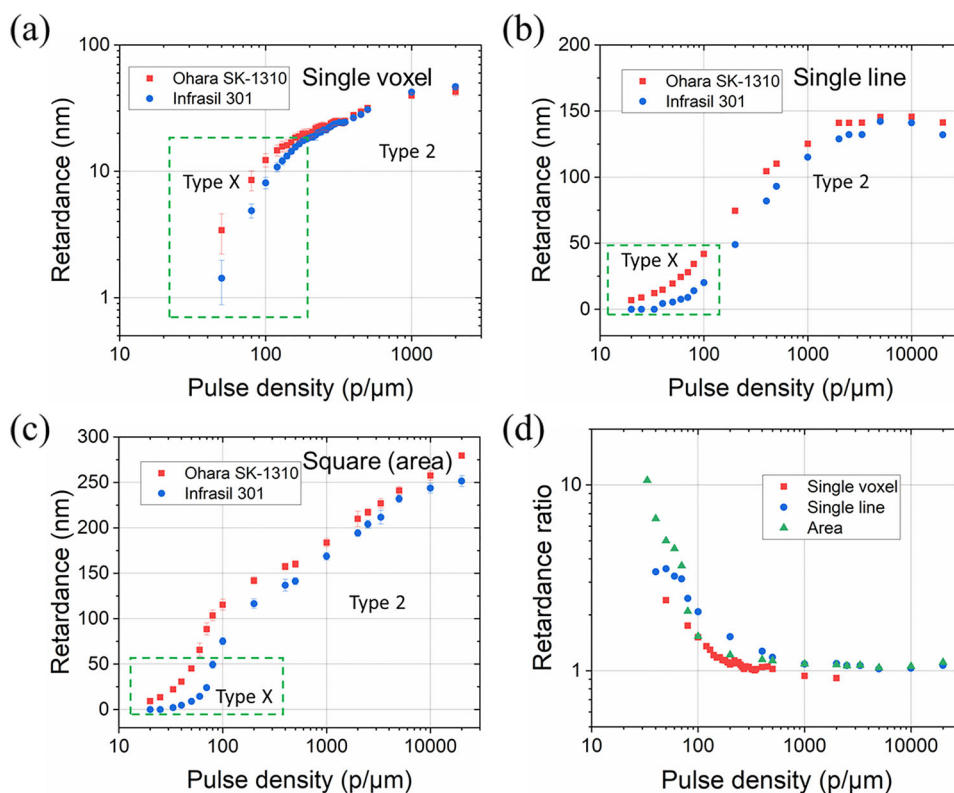


**Figure 4.** Material dependence of birefringent modification for the VAD sample (Ohara SK-1310) and electric fusion sample (Infrasil 301). a) Retardance of birefringent single voxel as a function of pulse density. b,c) Retardance of single line and area versus pulse density. d) The retardance ratio of birefringent modification versus pulse density between the VAD and the electrically fused sample.

case. However, the difference in the retardance of type 2 voxels, like the area scan, does not exceed 10%.

Similar tendencies can be observed for single line 4b writing in Ohara SK-1310 and Infrasil 301. The strongest difference in retardance values, which is up to 3.4 times, under the same writing conditions for type X modifications is observed (Figure 4b). However, only 10% retardance difference is revealed at higher pulse densities for type 2 structures. It should be noted that when scanning the area at the same pulse density (80 pulses  $\mu\text{m}^{-1}$ ), the Ohara SK-1310 and Infrasil 301 samples produce modifications of type 2 with a retardance of 110 nm and type X with 49 nm, respectively (Figure 4c). The ratio of retardance values in VAD (Ohara SK-1310) and electrically fused silica (Infrasil 301) samples as a function of pulse density was compared for different scanning geometries (Figure 4d). For type X voxels, the retardance ratio decreases from about 2 to 1 with increasing number of pulses, when type 2 modification appears. The largest material retardance ratio for single-line writing is around 3.4, and for area-sweep writing is close to 10, suggesting a strong material dependency of type X modification. On the other hand, the material retardance coefficient for modification based on nanogratings is close to unity for all writing geometries, which indicates a weak dependence on the material.

Moreover, we compared the isotropic refractive index increase (type 1 modification) in different grades of silica glass as well. In this case, a pulse duration of 190 fs was chosen to prevent the birefringent modification associated with nanograting formation

(Figure 5a). Indeed, no detectable birefringent modification was observed in the VAD (Suprasil 3302) and the electrically fused (Infrasil 301) samples. Quantitative phase imaging of the electrically fused sample revealed the optical path difference of about 1.3 times larger than that in the VAD sample subjected to the same irradiation conditions with the pulse energy of 0.9  $\mu\text{J}$  and the scanning speed of 5  $\text{mm s}^{-1}$  (Figure 5b). The corresponding refractive index change is estimated at  $6.2 \times 10^{-4}$  and  $4.8 \times 10^{-4}$  in samples Infrasil 301 and Suprasil 3302, respectively.

The mechanism of the observed difference in the modifications in different grades of silica glass can be explained as follows. Recently the observation of increased nanopore formation in silica glass when writing with elliptical polarization has been interpreted in terms of defects with low excitation energy, which have smaller band gap energy, promoting the formation of nanopores in the X-type modification.<sup>[42]</sup> One example of such defects with absorption at 2 eV is non-bridging oxygen-hole centers (NBO-HCs,  $\equiv\text{Si}-\text{O}\cdot$ ), which are formed during nonlinear photoionization of silica glass.<sup>[43,44]</sup> Other common defects with low excitation energy are self-trapped holes (STHs, hole-based polaron), which result in the radiation-induced absorption in a wide spectral region ranging from 0.6–2.6 eV in silica glass.<sup>[45,46]</sup> According to electron paramagnetic resonance analysis, two types of STH are present in irradiated silica: STH1 consisting of a hole localized on the non-bonding p-orbital of a single bridging oxygen atom in the silica network, and STH2 where hole is delocalized over (or tunneling between) two non-bonding p-orbitals

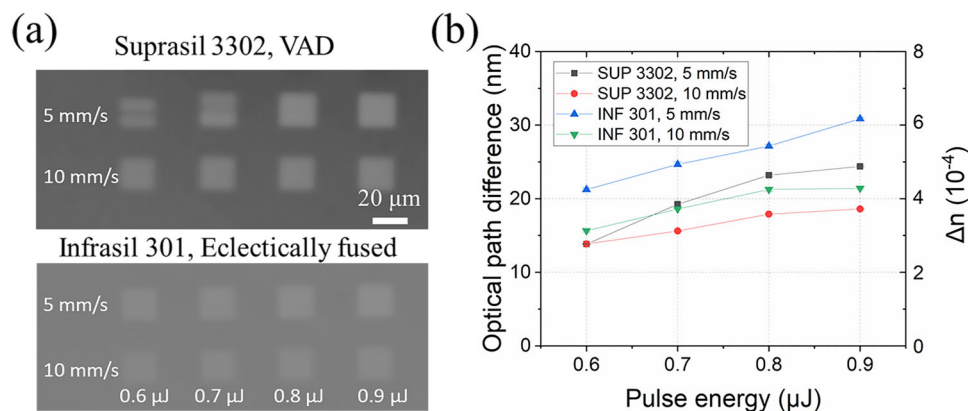


**Figure 5.** Material dependence of refractive index increase (type 1) for the VAD sample (Suprasil 3302) and electrically fused sample (Infrasil 301). a) Optical phase image of laser written areas in two samples. b) Optical phase difference and refractive index change in two samples versus writing pulse energies. Solid lines are guides for the eye. Processing conditions: 0.6–0.9 μJ pulse energy, 190 fs pulse duration, 5 or 10 mm s<sup>-1</sup> translation speed, and 0.16 NA aspheric lens.

of two neighboring bridging oxygen atoms of the same SiO<sub>4</sub> tetrahedron.<sup>[47]</sup> STHs are divided into two classes – inherent and strain-assisted. Inherent STHs occur at the network sites with normal, increased, or slightly reduced Si–O bond length. Strain-assisted STHs arise at the sites with a significantly reduced Si–O bond length. The STHs with the two bands at 1.88 and 1.63 eV are classified as strain assisted, STHs with the bands at 2.60 and 2.16 eV, as inherent. It was also assumed that the band at ≈0.6–0.7 eV (known as “low-temperature infrared absorption”) and the band at ≈1 eV were associated with inherent STHs. For a shortened Si–O bond, the electron cloud of the silicon is closer to the hole-containing oxygen which prolongs the STH lifetime and increases its thermal stability.

STHs and NBOHCs are produced and accumulated when glass is irradiated with a series of intense light pulses with a wavelength of 1030 nm. Subsequent pulses can excite STHs by tunneling, which results in activation of holes. Activation of hole-based polarons can possibly lead to clustering, which minimizes the energy of interaction between positive holes and the lattice, and then promotes the formation of nanopores. The low retardance of type X modification in the electric fusion sample can be explained by the higher concentration of ODCs, which may trap holes and prevent the nanopores formation.

ODCs are also produced in the regime of type 1 modification which is characterized by an isotropic refractive index increase in silica glass.<sup>[28]</sup> To validate the proposed explanation, we carried out an overwriting experiment in the VAD silica glass sample. E' centers (≡Si•) and ODC defects were first created in the sample by writing under conditions of type 1 modification (190 fs pulse duration, 0.7 μJ pulse energy, 10–40 mm s<sup>-1</sup> scanning speed, 200 kHz repetition rate), followed by overwriting under the conditions for type X modification (300 fs pulse duration, 0.7 μJ pulse energy, 6 mm s<sup>-1</sup> scanning speed, 200 kHz repetition rate) (Figure 6a). Square regions of 20 × 20 μm<sup>2</sup> were written at different scanning speeds which resulted in a higher defect concentration at a lower speed. The increase of retardance of type X modification was accompanied with decrease of the optical phase change produced by isotropic index change of type 1 modification (Figure 6b). The maximum retardance of about 10 nm for

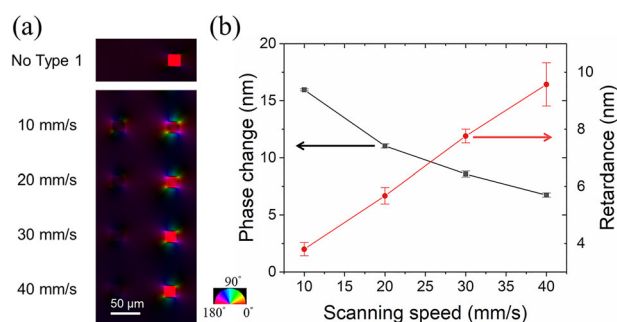


**Figure 6.** Overwrite type X on type 1 regions. a) Birefringent image of type 1 modifications (190 fs pulse duration, 0.7 μJ pulse energy, 10–40 mm s<sup>-1</sup> scanning speed) and overwritten by type X modifications (300 fs pulse duration, 0.7 μJ pulse energy, 6 mm s<sup>-1</sup> scanning speed). b) Phase change of type 1 modifications and retardance of overwritten type X squares versus scanning speed. Solid lines are guides for the eye.

type X structures after overwriting procedure is significantly less than 25 nm for structures written in pristine silica glass, suggesting that created defects prevent the formation of anisotropic nanopores and reduce the induced birefringence.

We also investigated laser writing in silica glass samples (Table 1, group B) manufactured with a few different treatments: a PCVD sample with low ODC defect concentration was fabricated by plasma CVD; sample 210BA is a VAD silica glass loaded with hydrogen, which passivates defects such as E' centers and increases UV absorption; sample 210B6 is a silica glass doped with fluorine (F), which decreases refractive index and increases the defect concentration;<sup>[48]</sup> sample 210B8 is a synthetic silica glass dried with an organosilicon compound, which results in low OH content and high concentration of defects (E' centers and ODCs). The writing parameters (300 fs pulse duration, 0.6 μJ pulse energy, 200 kHz repetition rate, 6 mm s<sup>-1</sup> scanning speed) were the same for all the samples. Interestingly, the retardance associated with the induced birefringence of X-type in the PCVD sample (Figure 7a, middle left) was as high as in the untreated VAD sample (Figure 7a, left), confirming the critical role of ODCs in preventing nanopores formation.

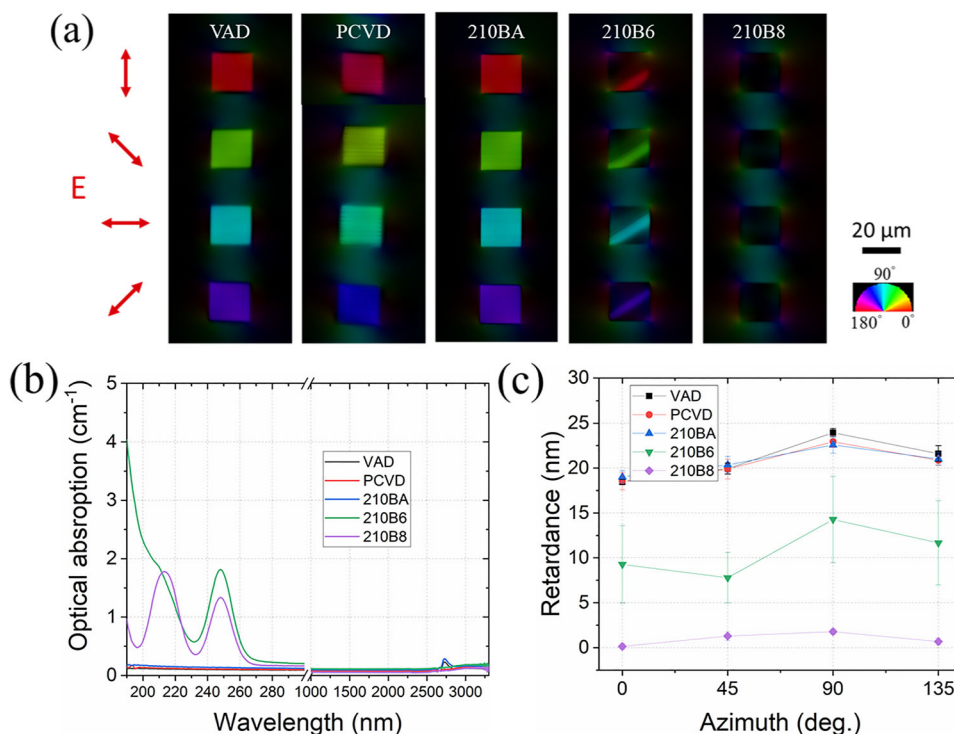


**Figure 7.** Laser writing inside different silica glasses. The 210BA is a VAD sample with loaded H<sub>2</sub>, the 210B6 is a F-doped silica glass and the 210B8 is a synthetic silica glass with a lot of defects. a) Birefringence images of laser-written regions. b) Optical absorption of five silica glass samples. c) Measured retardance of laser imprinted regions in different samples with the same laser writing parameters. Solid lines are guides for the eye. Processing conditions: 0.6 μJ pulse energy, 300 fs pulse duration, 6 mm s<sup>-1</sup> translation speed, and 0.16 NA aspheric lens.

The retardance of type X modification in the VAD sample (210BA) with passivated E' centers is very close to that in the VAD sample without hydrogen loading, which indicates an insignificant effect of the E' centers on the formation of anisotropic nanopores (Figure 7a, middle). In addition, a spatially non-uniform distribution of birefringent modification was observed in 210B6 silica glass, correlated with the non-uniform distribution of fluorine in this sample, in which higher retardance occurs in regions with lower F concentration (Figure 7a, middle right). The stronger retardance can be attributed to lower defect concentration associated with lower fluorine concentration. It should be noted that the defect concentration is not directly dependent on the F concentration and the manufacturing process is more important for defects formation in silica glass. In addition, no birefringent modification was detected in the 210B8 sample (Figure 7a, right), which could further confirm our interpretation. Due to some residual carbon and a very high concentration of ODCs in sample 210B8, its viscosity and concentration of strained bonds can be higher than in conventional synthetic silica glass, resulting in deeper hole traps and lower hole mobility, which prevents the formation of anisotropic nanopores. The optical absorption of five samples was measured in the range from ultraviolet to infrared. The absorption of ODC (II) (Si: or twofold coordinated silicon) at 248 nm was observed in 210B6 and 210B8 samples, whereas this absorption was absent in the VAD, PCVD, and 210BA samples, indicating a much lower defect concentration (Figure 7b). Since the absorption at 248 nm is similar for 210B6 and 210B8, the concentration of ODC(II) is close in

both samples. However, the retardance of type X modification in the 210B8 is smaller than that of 210B6, implying that the ODC (I) ( $\equiv\text{Si}-\text{Si}\equiv$ , oxygen vacancy), which has the absorption peak at 163 nm, contributes more to the observed material dependence. The concentration of ODC (I) is typically 10<sup>2</sup>–10<sup>3</sup> times higher than ODC (II)<sup>[49]</sup> and the minimum birefringence in the 210B8 sample can be attributed to the highest concentration of ODC (I) due to drying with an organosilicon compound. In the VAD sample, the retardance of laser-written regions was about 20 nm, while in 210B6 it was  $\approx 10$  nm with a maximum deviation due to the non-uniform distribution of fluorine and defects (Figure 7c).

In addition, another set of silica glass samples was used to further confirm our interpretation (Table S2, Supporting Information): “Wet” is a Suprasil 2 synthetic silica glass with high amount of OH; F7C is silica glass doped with fluorine with a concentration of 3.23%; LBL and L552 are dry VAD silica glass samples with high ODC concentration. From this set of glasses, wet silica samples showed a slightly higher value of X-type retardance than in F7S, LBL, and L552 silica glasses with a higher ODC concentration, which is still lower than in the previously described organosilicon compound dried 210B8 silica glass.

Laser-induced ultra-high transmittance birefringence in silica glass is used for the fabrication of geometric phase optical elements and vector beam converters. Reducing the fabrication time is one of the main challenges in this application. According to the previous conclusion, with the same writing parameters the retardance of type X modification is the largest in VAD samples. But the difference can be compensated by using larger pulse energy

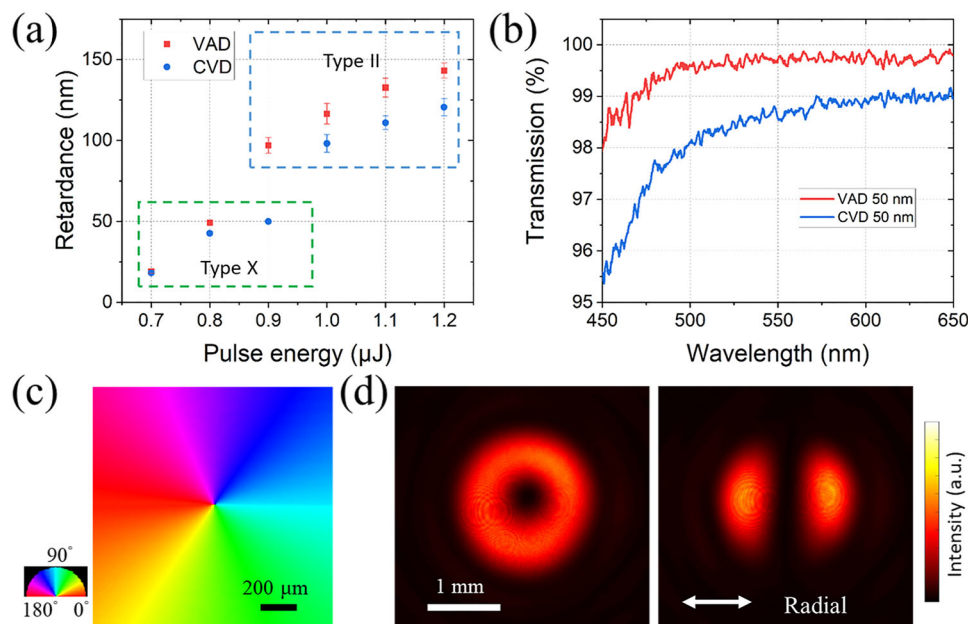


**Figure 8.** Vector beam converter imprinted with high transmission birefringent modification. a) Retardance as a function of pulse energy in VAD and CVD silica glass samples. The pulse duration was 600 fs, and the scanning speed is  $8 \text{ mm s}^{-1}$ . b) Transmission of birefringent square with the same retardance of 50 nm in two samples, where the pulse energy is 0.8 (0.9)  $\mu\text{J}$  for the VAD (CVD) sample. c) Birefringence image of the center part of the vector beam converter imprinted in a VAD sample. d) Far-field intensity pattern of a 515 nm radially polarized laser beam after converter without (left) and with (right) a polarizer.

or lower scanning speed in a CVD sample. For example, the retardance of type X modification in the CVD sample written by 0.9  $\mu\text{J}$  pulses is close to that fabricated by 0.8  $\mu\text{J}$  pulses in the VAD sample (Figure 8a), while the pulse duration is 600 fs, and the scanning speed is  $8 \text{ mm s}^{-1}$ . However, the advantage of the type X birefringence modification in the VAD sample is higher visible transmission compared to CVD glass at the same retardance, e. g. of 50 nm (Figure 8b). The difference in transmission is especially noticeable at shorter wavelengths, 98% and 95.5% at 450 nm in the VAD and CVD samples, respectively, with the same 50  $\mu\text{m}$  thickness of birefringent layer.

For demonstration purposes, we fabricated an ultra-high transmittance vector beam converter in a VAD silica glass sample. The converter is a space variant half waveplate with slow axis orientation linearly changing from  $0^\circ$  to  $180^\circ$  with respect to the azimuth (Figure 8c), which generates a radially or azimuthally polarized vector beam from an incident linearly polarized beam.<sup>[23]</sup> To achieve a half-wave retardance of 257 nm, 6 birefringent layers were imprinted with 600 fs pulses, an energy of 0.8  $\mu\text{J}$  and a scanning speed of  $8 \text{ mm s}^{-1}$ . The measured retardance difference in type X structures written with polarizations parallel and perpendicular to the scanning direction was less than 5%, which is less than the typical 15–20% for the structures based on nanogratings. A radially polarized beam with a donut-shaped intensity distribution was measured in the far-field (Figure 8d, left), which was confirmed by a double-lobed intensity pattern with a linear polarizer (Figure 8d, right).

We also investigated 5D optical data storage based on ultra-high transmittance birefringent modification (type X) in different grades of silica glass. The matrix of data voxels with a separation

of 2  $\mu\text{m}$  was imprinted in a VAD silica glass sample (Ohara SK-1310) (Figure 9a) and an electrically fused sample (Infrasil 301) (Figure 9b). Since the 5.7  $\mu\text{m}$  beam diameter was larger than the 2  $\mu\text{m}$  inter-voxel spacing, the slow axis azimuth of some of the data voxels in the Ohara SK-1310 silica glass was affected by subsequent laser pulses from the neighboring voxel. In contrast, due to smaller modification size, the slow axis azimuth of voxels in the Infrasil 301 sample was less affected by the pulses writing nearby voxels, which results in higher azimuth accuracy.

An azimuthal birefringence error of  $1.1^\circ$  and  $0.9^\circ$  is estimated in Ohara SK-1310 and Infrasil 301 respectively for voxels imprinted with 150 pulses and 5  $\mu\text{m}$  spatial separation, which means no overwriting effects between voxels and eight azimuths data storage with 100% readout accuracy can be realized in both samples (Figure 9c). To achieve higher data capacity, the distance between voxels was reduced to 2  $\mu\text{m}$  and the lower azimuth error was observed in the Infrasil 301 silica glass with the pulse number varied from 80 to 150 (Figure 9d). For example, the error of slow axis orientation for voxels written by 120 pulses was 3.3 degrees in the Infrasil 301 silica glass and 5.2 degrees in the Ohara SK-1310 sample. Therefore, the 100% data readout accuracy can only be achieved in the Infrasil 301 silica glass for high density data storage in the regime of anisotropic nanopore formation, which will be reported elsewhere. More specifically, the capacity of type X based data storage in Infrasil 301 silica glass is about 700 GB per disc, higher than 350 GB of the same size Ohara SK-1310 glass. In addition, the manufacturing cost of electrically fused quartz is only half that of VAD silica glass, so the cost of optical discs in 5D data storage can be significantly reduced by using the former.

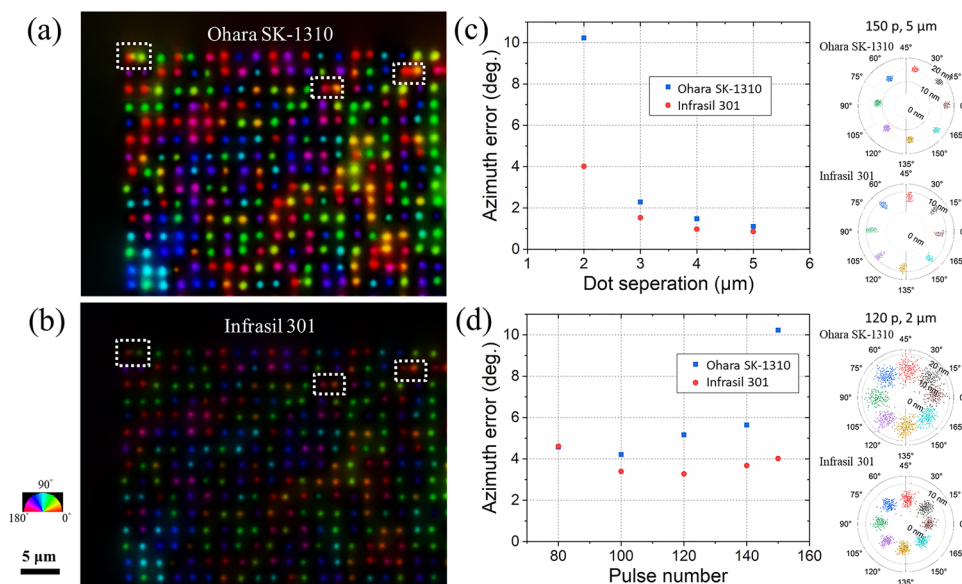


**Figure 9.** Multiplexed data storage in different silica glasses. Birefringence images of imprinted voxels in silica glass of a) Ohara SK-1310 and b) Infrasil 301, respectively. The data voxels were written by 150 pulses with the voxel separation of 2  $\mu\text{m}$ . c) Azimuth error of birefringent voxels with different dot separation and writing pulse number of 150. d) Azimuth error of birefringent voxels with different writing pulse numbers and 2  $\mu\text{m}$  dot separation. Two inset images show polar distribution of azimuth and retardance of voxels in Ohara SK-1310 (top) and Infrasil 301 (bottom) samples. Processing conditions: 0.7  $\mu\text{J}$  pulse energy, 300 fs pulse duration, 1  $\text{mm s}^{-1}$  translation speed, and 0.16 NA aspheric lens.

### 3. Conclusion

In conclusion, we demonstrated the dependence of ultrafast laser writing in silica glass on the method of its manufacture. While difference in birefringence for nanograting based modification (type 2) was less than 10%, it was five times stronger for nanopores-based modification (type X) in the VAD glass compared to the electrically fused silica sample with the same writing parameters. Moreover, 30% stronger refractive index increase (type 1) was observed in silica glass produced by melting of natural quartz crystals. The difference of ultrafast laser writing in different grades of silica glass is explained by higher concentration of ODCs, in particular ODC (I) ( $\equiv\text{Si}-\text{Si}\equiv$ ) in fused quartz, which trap STHs and prevent their clustering and the formation of nanopores. On the other hand, ODCs can promote compaction in silica glass resulting in increase of refractive index. In addition, the difference in the strength of modifications imprinted by different writing patterns was interpreted in terms of free carrier diffusion leading to a decrease of space charge field and an increased concentration of hole-based defects in line scanning compared to voxel pattern writing. The observed dependence of ultrafast laser nanostructuring has been exploited for efficient fabrication of vector beam converters in the VAD glass and low cost 5D optical data storage with higher capacity and readout accuracy in electrically fused silica glass.

### 4. Experimental Section

The laser writing experiments were carried out with a Yb:KGW femtosecond laser system (PHAROS, Light Conversion Ltd.), operating at 1030 nm and delivering pulses with 200 kHz repetition rate and tunable duration from 190 to 600 fs. The laser beam was focused via a 0.16 NA aspheric lens 170  $\mu\text{m}$  beneath the surface of sample, which was mounted

on a XYZ linear air-bearing translation stage (Aerotech Ltd.). The sample translation speed varied from 0.1 to 6  $\text{mm s}^{-1}$ , which corresponded to a pulse density of 2000 and 33 pulses per micron, and the distance between the lines was fixed at 1  $\mu\text{m}$ . It should be noted that the degree of material modification depended on the deposited energy and was determined by the density of pulses. Pulse density for line and area raster scanning was defined as the number of pulses deposited within the size of the material modification spot, which for type X was measured at about 1  $\mu\text{m}$  and was significantly smaller than the laser spot size of 5.7  $\mu\text{m}$  for 0.16 NA focusing lens due to nonlinearity of the process. The polarization azimuth of the laser beam was controlled by a combination of a polarizer, an electro-optic modulator, and a quarter wave-plate. The retardance and slow axis orientation of the birefringent modifications were quantified using a birefringence measurement system (CRi Abrio imaging system) operating at 546 nm and built into an Olympus BX51 optical microscope. The retardance was the product of the birefringence of the structure and the longitudinal length of the structure, which reads  $\text{Ret.} = \Delta n_b \times l$ . The refractive index changes were characterized with a wavefront sensor (SID4-HR, Phasics) mounted on the same microscope.

### Supporting Information

Supporting Information is available from the Wiley Online Library or from the author.

### Acknowledgements

The study was supported by the European Research Council (ENIGMA, grant No. 789116), the Microsoft (Project Silica), Horizon 2020 RISE Project (CHARTIST, 101007896), and the Academy of Finland (343393, 320166).

### Conflict of Interest

The authors declare no conflict of interest.

## Data Availability Statement

The data that support the findings of this study are available from the corresponding author upon reasonable request.

## Keywords

defects, free carrier diffusion, silica glass, ultrafast laser writing

Received: December 13, 2022

Revised: January 19, 2023

Published online:

- [1] A. Vogel, J. Noack, G. Hüttman, G. Paltauf, *Appl. Phys. B* **2005**, *81*, 1015.
- [2] A. Ródenas, M. Gu, G. Corrielli, P. Paiè, S. John, A. K. Kar, R. Osellame, *Nat. Photonics* **2019**, *13*, 105.
- [3] X.-L. Zhang, F. Yu, Z.-G. Chen, Z.-N. Tian, Q.-D. Chen, H.-B. Sun, G. Ma, *Nat. Photonics* **2022**, *16*, 390.
- [4] K. Sugioka, Y. Cheng, *Light: Sci. Appl.* **2014**, *3*, e149.
- [5] A. Marcinkevičius, S. Juodkazis, M. Watanabe, M. Miwa, S. Matsuo, H. Misawa, J. Nishii, *Opt. Lett.* **2001**, *26*, 277.
- [6] Y. Bellouard, A. Said, M. Dugan, P. Bado, *Opt. Express* **2004**, *12*, 2120.
- [7] C. Hnatovsky, R. Taylor, E. Simova, V. Bhardwaj, D. Rayner, P. Corkum, *Opt. Lett.* **2005**, *30*, 1867.
- [8] E. Glezer, M. Milosavljevic, L. Huang, R. Finlay, T.-H. Her, J. P. Callan, E. Mazur, *Opt. Lett.* **1996**, *21*, 2023.
- [9] P. Zijlstra, J. W. Chon, M. Gu, *Nature* **2009**, *459*, 410.
- [10] S. M. Eaton, H. Zhang, P. R. Herman, F. Yoshino, L. Shah, J. Bovatsek, A. Y. Arai, *Opt. Express* **2005**, *13*, 4708.
- [11] Y. Liao, J. Ni, L. Qiao, M. Huang, Y. Bellouard, K. Sugioka, Y. Cheng, *Optica* **2015**, *2*, 329.
- [12] B. Zhang, D. Tan, Z. Wang, X. Liu, B. Xu, M. Gu, L. Tong, J. Qiu, *Light: Sci. Appl.* **2021**, *10*, 93.
- [13] K. Sun, D. Tan, X. Fang, X. Xia, D. Lin, J. Song, Y. Lin, Z. Liu, M. Gu, Y. Yue, *Science* **2022**, *375*, 307.
- [14] D. Wei, C. Wang, H. Wang, X. Hu, D. Wei, X. Fang, Y. Zhang, D. Wu, Y. Hu, J. Li, *Nat. Photonics* **2018**, *12*, 596.
- [15] T. Xu, K. Switkowski, X. Chen, S. Liu, K. Koynov, H. Yu, H. Zhang, J. Wang, Y. Sheng, W. Krolikowski, *Nat. Photonics* **2018**, *12*, 591.
- [16] A. Mermillod-Blondin, C. Maclair, A. Rosenfeld, J. Bonse, I. V. Hertel, E. Audouard, R. Stoian, *Appl. Phys. Lett.* **2008**, *93*, 021921.
- [17] M. Lancry, B. Pommellec, J. Canning, K. Cook, J. C. Poulin, F. Brisset, *Laser Photonics Rev.* **2013**, *7*, 953.
- [18] E. Casamenti, S. Pollonghini, Y. Bellouard, *Opt. Express* **2021**, *29*, 35054.
- [19] R. Brueckner, *J. Non-Cryst. Solids* **1970**, *5*, 123.
- [20] K. M. Davis, K. Miura, N. Sugimoto, K. Hirao, *Opt. Lett.* **1996**, *21*, 1729.
- [21] Y. Shimotsuma, P. G. Kazansky, J. Qiu, K. Hirao, *Phys. Rev. Lett.* **2003**, *91*, 247405.
- [22] V. R. Bhardwaj, E. Simova, P. P. Rajeev, C. Hnatovsky, R. S. Taylor, D. M. Rayner, P. B. Corkum, *Phys. Rev. Lett.* **2006**, *96*, 057404.
- [23] M. Beresna, M. Gecevičius, P. G. Kazansky, T. Gertus, *Appl. Phys. Lett.* **2011**, *98*, 201101.
- [24] C. Hernández-García, A. Turpin, J. San Román, A. Picón, R. Drevinskas, A. Cerkauskaitė, P. G. Kazansky, C. G. Durfee, Í. J. Sola, *Optica* **2017**, *4*, 520.
- [25] Y. Fang, M. Han, P. Ge, Z. Guo, X. Yu, Y. Deng, C. Wu, Q. Gong, Y. Liu, *Nat. Photonics* **2021**, *15*, 115.
- [26] Y. Shimotsuma, M. Sakakura, P. G. Kazansky, M. Beresna, J. Qiu, K. Miura, K. Hirao, *Adv. Mater.* **2010**, *22*, 4039.
- [27] J. Zhang, M. Gecevičius, M. Beresna, P. G. Kazansky, *Phys. Rev. Lett.* **2014**, *112*, 033901.
- [28] M. Sakakura, Y. Lei, L. Wang, Y. H. Yu, P. G. Kazansky, *Light: Sci. Appl.* **2020**, *9*, 15.
- [29] H. Wang, Y. Lei, L. Wang, M. Sakakura, Y. Yu, G. Shayeganrad, P. G. Kazansky, *Laser Photonics Rev.* **2022**, *16*, 2100563.
- [30] Y. Lei, M. Sakakura, L. Wang, Y. Yu, H. Wang, G. Shayeganrad, P. G. Kazansky, *Optica* **2021**, *8*, 1365.
- [31] I. Fanderlik, *Silica Glass and Its Application*, Elsevier, Amsterdam **2013**.
- [32] M. Lancry, N. Grothoff, S. Guizard, W. Yang, B. Pommellec, P. Kazansky, J. Canning, *J. Non-Cryst. Solids* **2009**, *355*, 1057.
- [33] M. Lancry, J. Canning, K. Cook, M. Heili, D. Neuville, B. Pommellec, *Opt. Mater. Express* **2016**, *6*, 321.
- [34] F. Zimmermann, M. Lancry, A. Plech, S. Richter, B. H. Babu, B. Pommellec, A. Tünnermann, S. Nolte, *Opt. Lett.* **2016**, *41*, 1161.
- [35] S. Richter, C. Miese, S. Döring, F. Zimmermann, M. J. Withford, A. Tünnermann, S. Nolte, *Opt. Mater. Express* **2013**, *3*, 1161.
- [36] S. Fedotov, R. Drevinskas, S. Lotarev, A. Lipatiev, M. Beresna, A. Čerkauskaitė, V. Sigaev, P. Kazansky, *Appl. Phys. Lett.* **2016**, *108*, 071905.
- [37] V. Niziev, A. Nesterov, *J. Phys. D: Appl. Phys.* **1999**, *32*, 1455.
- [38] A. Patel, V. T. Tikhonchuk, J. Zhang, P. G. Kazansky, *Laser Photonics Rev.* **2017**, *11*, 1600290.
- [39] A. Collins, D. Rostohar, C. Prieto, Y. Chan, *Opt. Lasers Eng.* **2014**, *60*, 18.
- [40] E. M. Dianov, P. Kazanskiĭ, D. Y. Stepanov, *Quantum Electron.* **1989**, *19*, 575.
- [41] D. Z. Anderson, V. Mizrahi, J. E. Sipe, *Opt. Lett.* **1991**, *16*, 796.
- [42] Y. Lei, G. Shayeganrad, H. Wang, M. Sakakura, Y. Yu, L. Wang, D. Kliukin, L. Skuja, Y. Svirko, P. G. Kazansky, *Light: Sci. Appl.* **2023**.
- [43] L. Skuja, *J. Non-Cryst. Solids* **1998**, *239*, 16.
- [44] R. Stoian, K. Mishchik, G. Cheng, C. Maclair, C. D'Amico, J.-P. Colombier, M. Zamfirescu, *Opt. Mater. Express* **2013**, *3*, 1755.
- [45] D. L. Griscom, *Phys. Rev. B* **1989**, *40*, 4224.
- [46] D. L. Griscom, *J. Non-Cryst. Solids* **2006**, *352*, 2601.
- [47] P. F. Kashaykin, A. L. Tomashuk, M. Y. Salgansky, A. N. Guryanov, E. M. Dianov, *J. Appl. Phys.* **2017**, *121*, 213104.
- [48] J. W. Fleming, D. L. Wood, *Appl. Opt.* **1983**, *22*, 3102.
- [49] L. Skuja, M. Hirano, H. Hosono, K. Kajihara, *Phys. Status Solidi C* **2005**, *2*, 15.